Received: 8 October 2023 | Revised: 12 December 2023 | Accepted: 15 December 2023 | Published online: 20 December 2023

RESEARCH ARTICLE

Epilepsy Detection by Different Modalities with the Use of AI-assisted Models

Artificial Intelligence and Applications

yyyy, Vol. XX(XX) 1–5

DOI: 10.47852/bonviewAIA32021848

BON VIEW PUBLISHING

Jayanthi Vajiram[1,*], Sivakumar.S[1], Roanek Jena[1] and Utkarsh Maurya[1]

1 Vellore Institute of Technology, India

Abstract: Epilepsy is characterized by recurrent seizures originating from any four brain lobes. It includes focal seizures with symptoms of alterations in consciousness, and cognitive impairments, including memory and language difficulties. It must be radiologically identified by proper diagnosis and course of therapy. However, a visual inspection of images may not always yield an accurate interpretation from radiologists, necessitating AI-assisted methods. The computer-vision-based radiological methods are used to enhance the treatment of epilepsy by image bio-markers and deep learning algorithms. These methods are used to predict disease progression and treatment. It specifies the focus of the research on epilepsy detection using new U-TRGN classification models. These models used for lateralization and localization of brain activity in this process. This study gives the idea of pre-operative findings of different imaging modalities and post-operative findings of EEG data analysis. The data has been pre-processed through normalization, smoothing, and noise removal techniques. The data is then classified using U-transfer reinforced gaussian networks (U-TRGN), after feature selection by kernel Convolutional analysis (KCA). The performance metrics are evaluated through the training accuracy, validation accuracy, precision, Dice coefficient, and area under a region of the convergence curve. The proposed technique attained an accuracy of 97.04%, precision of 94.12%, dice coefficient of 2.96%, and AUC of 99.56% which is better than the existing methods and it will be a baseline for upcoming studies.

Keywords: epilepsy, new U-TRGN model, KCA algorithm, deep learning models

***Corresponding author:** Jayanthi Vajiram, Vellore Institute of Technology, India. Email: jayanthi.2020@vitstudent.ac.in

1. Introduction

The epilepsy is a neurological disorder and a non-communicable disease [1]. The abnormality occurs, when the electrical activity of brain disrupts a part or entire body with sudden seizures. Around 60 million people worldwide suffer from a variety of epileptic seizures. These epilepsies affect static memory, and cognitive abilities that can make serious brain injury to the patient. The patient experience trouble in normal communication with society, which leads to the humiliation and absence of fitting societal position. They are treated by different modalities and also by using MRI guided stereotactic laser interstitial thermal therapy [2]. Thus, early recognition of epileptic seizures can help patients to lead quality life. Treatment procedures are carried by checking the neuroimaging modalities and case history [3,4]. EEG data can provide valuable insights into the lateralization and localization of brain activity of the patients. Lateralization shows either the left or right hemisphere of the brain activities. In the context of epilepsy detection, lateralization can help determine which hemisphere of the brain is primarily affected by abnormal electrical activity. Localization refers to the specific brain regions or areas that are involved in epileptic seizures. The various diagnostic tests, including Electrocorticography (ECoG), magnetoencephalography (MEG), positron emission tomography (PET), single-photon emission computed tomography (SPECT), functional MRI (fMRI), functional near-infrared spectroscopy (fNIRS)

methods [5]. The abnormalities are widespread throughout the brain, and to identify the brain region by manual annotation of individual scans gives 5 to 10% error. The 86% of affected cases were overlooked, according to earlier study [6]. For instance, one-third of healthy adults have unilaterally enlarged temporal horns and aberrant hippocampal signaling visible on fluid-attenuated inversion recovery (Flair) and T2-weighted imaging. Convolutional neural networks (CNNs) are a group of profound learning method, which gives better execution of features and characters in the dataset. A machine learning classifier of SVM (support vector machine), DBN (deep belief network), KNN (k-nearest neighbor), RF (random forest), DNN (deep neural network) and U-TGN could be used to solve this issue. The classifier models have a bunch of processing methods, and the results of detecting epilepsy supports to minimize the medical procedure. The classification models, which gives hidden or obscure factors in data, and may provide more accurate outcomes compared to the old statistical methods [7]. The postoperative seizure control imaging investigations offer predictions of individual patient outcomes and relationship across entire cohorts and gives significant advancement in personalized patient care. This study explains the classification models used to detect abnormal brain activity patterns through lateralization and localization information, and achieve higher accuracy in detecting and localizing epileptic seizures.

2. Literature Review

The cognitive deterioration can occur in 70-80% of cases, and this is influenced by various epilepsy-related features [8]. Long-term epilepsy-associated tumors are typically low-grade, slowly growing tumors located in the cortex, and they primarily affect young patients with family medical histories of epilepsy [9]. Epilepsy gives noticeable effects on behavior, and cognitive abilities. Evidence proves that epilepsy can also impact behavior as observed through structured interviews assessing through five-factor model of personality test [10]. Studies of epilepsy proved with sleep disturbances using the trail making test [11]. Correlations between changes in neuropsychological test scores and brain metabolism have been explored using statistical parametric mapping, which indicates metabolic changes by the Boston Naming Test [12]. Volumetric MRI identifies epilepsy progression of brain atrophy [13]. The single-voxel spectroscopy has been used to compare children with different seizure types and to differentiate patients with intractable and non-intractable epilepsy [14]. To diagnose and categorize the epilepsy, machine learning techniques gives effective analysis of discriminative characteristics generated from brain pictures, with SVMs classifiers on the MRI data [15], and Diffusion Tensor Imaging (DTI) data of individuals with mesial temporal lobe epilepsy [16]. Quantitative relaxometry as well as DTI data were used with SVM [17] to enhance the identification of temporal lobe epilepsy. The CNN classifier are used for histopathological assessment of WSI images to recognize different subtypes of Focal Cortical Dysplasia with hyperplasia in epilepsy cases [18]. The nocturnal frontal lobe epilepsy was analyzed with two-dimensional self-organizing maps, which used to cluster the data into seizure and non-seizure patterns [19]. The XAI4EEG system of data under time constraints significantly reduced the time needed to validate predictions and improved interpretability compared to SHAP feature contribution plots [20]. The SVM classifier detecting epileptic seizures in long-term EEG data [21]. EEG signals offer a solution for seizure prevention by classification performance scores of accuracies, AUC-ROC curve, sensitivity, and specificity [22]. The signal was analyzed to extract features for a classifier detecting activation and quiescent phases. The classifier's output was then applied to a finite state machine for cyclic alternating pattern method. The classifiers were tested using a sequential feature selection algorithm and principal component analysis [23]. The two decision forest classifiers, SysFor and Forest CERN, were applied to an ECoG brain dataset. The results showed that these classifiers significantly reduced seizure detection time while maintaining high accuracy. Additionally, they were able to identify the specific region of the brain most affected by seizures. FCM (fuzzy c-mean) and SVM methods were used to create an image segmentation method by combining the two preceding algorithms and testing its efficacy in a brain image with high bias and noise. Ontology-based heterogeneous feature detection with classifiers models also gives better results. Tus dataset from Temple University School of Medicine analyzed by six pre-trained models, namely Alex Net, GoogLeNet, Inception-v3, ResNet18, VGG16, and VGG19 used for seizure classifications [24-28]. DCLNN model was used to analyze the resection cavities on postsurgical epilepsy patient dataset [29]. Diffusion kurtosis tensor used to identity the epilepsy [30]. A comprehensive analysis of 190 studies revealed a growing preference for using Convolutional Neural Networks along with Time-Frequency decomposition method images. EEG signals with their subjective interpretation can sometimes result in misdiagnosis. To address this issue, this research paper introduces a deep learning model for seizure detection. The model employs a two-dimensional representation of EEG features and exhibits excellent scalability in neural networks. It demonstrates high applicability and accuracy in classifying seizures [31-34]. Microglial TRPV1 has been found to have a role in neuroinflammatory reactions, associated with seizures. Researchers have proposed a Takagi-Sugeno-Kang fuzzy system framework to classify epilepsy data, which can aid the treatment planning. Algorithm called MVTL-LSR, based on multi-view transfer learning, has been proposed to study epileptic EEG signals and enhance AI-assisted recognition of epilepsy. The SECNN-LSTM algorithm has shown effectiveness in predicting EEG signals related to epilepsy, leading to improved recognition rates for the disease. The prompt removal of artifacts from EEG signals is crucial to preserve the original signal features and ensure robust classification for accurate epilepsy detection by Google Net, VGG16, and Alex Net models with k- fold cross validation. The earlier study used the OAOFS-DBNECD technique, which transformed the signals into a .csv format. For the design of the epilepsy EEG analysis model, an Auto ML algorithm was utilized, which automatically generated a model based on the input data [35to 44].

2.1 Theoretical framework

2.1.1. Imaging modalities used in Epilepsy cases

The epilepsy studies were analyzed at the Cerebrum Imaging Centre using preoperative MRI data. This suggests that the center is using MRI scans to study epilepsy cases before the patients undergo surgery. This type of study can help identify abnormalities or specific regions in the brain that contribute to epileptic seizures.

Figure 1
Different imaging modalities of Epilepsy hypometabolism maps to resection regions

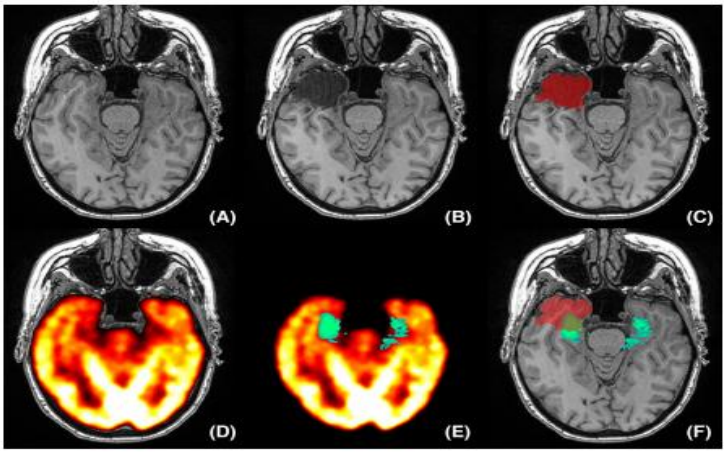

Figure 1 explains the epilepsy patient was analyzed before surgery by the use of (A) magnetic resonance imaging (MRI). (B) the post-op X-ray. (C) Segmented preoperative and postoperative MRIs were subtracted (red) to obtain the volume of the tissue that was removed. (D) MRI registration for FDG-PET (E) Comparison of hypometabolism to healthy controls (green). (F) Resection district overlay with hypometabolism (covered in green-light green), used to determine the amount of resected transient curve hypometabolism.

The data acquisition and imaging setup used at the Imaging Center. This included 3 T Siemens Magnetom Prisma-Fit furnished with a 64-channel head curl. Following a T1-weighted (T1w) structural scan, participants underwent resting-state functional MRI (rs-fMRI) and multi-shell diffusion-weighted imaging (DWI). In addition, two spin-echo images were taken to correct individual rs-fMRI scan distortion. Two T1w checks with indistinguishable boundaries were obtained with a 3D charge arranged fast inclination reverberation succession (MP-Fury; 0.8 mm isotropic voxels, lattice = 320 × 320, 224 sagittal cuts, (repetition time) TR = 2300 ms, (echo time) TE = 3.14 ms, TI = 900 ms, flip point = 9°, iPAT = 2, halfway Fourier = 6/8). Before being submitted for further processing, both T1w scans were visually examined to ensure that there was minimal head movement. qT1 relaxometry information were gained utilizing a 3D-MP2RAGE grouping (0.8 mm isotropic voxels, 240 sagittal cuts, TR = 5000 ms, TE = 2.9 ms, TI 1 = 940 ms, T1 2 = 2830 ms, flip point 1 = 4°, flip point 2 = 5°, iPAT = 3, data transfer capacity = 270 Hz/px, reverberation dividing = 7.2 ms, halfway Fourier = 6/8). We joined two reversal pictures for qT1 planning to limit aversion to B1 inhomogeneities and improve intra-and between subject reliability58,59. To obtain DWI data, a 2D spin-echo echo-planar imaging sequence with multi-band acceleration was used. The sequence consisted of three shells with b-values of 300, 700, and 2000s/mm2 and 10, 40, and 90 diffusion weighting directions per shell (1.6 mm isotropic voxels, TR = 3500 ms, TE = 64.40 ms, flip angle = 90°, refocusing flip angle = 180°, FOV = b0 pictures obtained backward stage encoding bearing are likewise accommodated mutilation adjustment of DWI examines. One 7 min rs-fMRI examine was gained utilizing multiband sped up 2D-Intense reverberation planar imaging (3 mm isotropic voxels, TR = 600 ms, TE = 30 ms, flip point = 52°, FOV = 240 × 240 mm2, cut thickness = 3 mm, mb factor = 6, reverberation separating = 0.54 ms). Members were told to keep their eyes open, take a gander at an obsession cross, and not nod off. To correct for distortion in the rs-fMRI scans, we also include two spin-echo images encoded in reverse phase (TR = 4029 ms, TE = 48 ms, flip angle = 90°, FOV = 240 240 mm2, echo spacing = 0.54 ms, phase encoding = AP/PA, bandwidth = 2084 Hz/Px). The timing difference between slices was adjusted after the scans were checked for significant head movement (more than 3 mm or 3°). The images were realigned to the middle slice after being spatially normalised to the MNI template. The automated anatomical labelling (AAL) atlas (23), used to segment the brain into 116 regions, includes 90 regions in the cerebrum and 26 regions in the cerebellum. These ROIs were used as nodes in the construction of the resting-state functional network. The comprehensive imaging protocol that comes with this data release contains the number of parameters used in the acquisition.

The data acquisition and imaging setup for FDG-PET epilepsy detection typically use the radiotracer, is a radioactive form of glucose that is injected into the patient's bloodstream, tracer travels through the body and is taken up by brain active cells of higher glucose metabolism, than scanning, imaging and analysis was captured.

2.1.2. Isotopes used in PET scans

Isotype	^{11}C	^{13}N	^{15}O	^{18}F	^{68}Ga	^{64}Cu	^{52}Mn	^{55}Co	^{9}Zr	^{82}Rb
Half-life	20min	10min	2min	110min	67.81min	12.7h	5.6day	17.5h	78.4h	1.3min

X-ray and CT scanning parameters gives the slice thickness, scan range, and radiation dose, and acquires a series of 2D images in axial, coronal, or sagittal planes. The X-ray beam rotates around the patient, capturing multiple images from different angles scan gives the detailed anatomical images of the brain, they may not always be sufficient for detecting certain types of epileptic activity. Additional imaging modalities with EEG is required in initial stage of epilepsy detection. CT scans helps to identify epilepsy related abnormalities or other brain lesions by very low range of 7% to 10% proved by NIH studies. Cylin-dependent kinase-like5 (CDKL5) genetic variation leads to the development of epileptic encephalopathy was recognized on 2004.

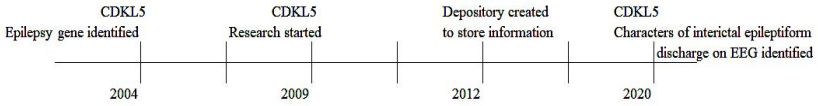

EEG used for early, and crucial during the surgical stage of epilepsy detection. In cases where medications fail to adequately control seizures, leads to surgery. EEG is used to precisely locate the seizure foci or the specific area in the brain responsible for generating seizures. This helps to perform surgical procedures to remove or disconnect the seizure focus. The different imaging modalities helps to compare the epilepsy symptoms and surgical intervention.

3. Research Methodology

3.1. Dataset details

The original dataset consists of 500 individuals, each with 4097 data points representing brain activity recorded over 23.6 seconds. The data is divided into 23 chunks, with each chunk containing 178 data points for 1 second. The last column of each chunk represents the label, with values ranging from 1 to 5 representing different conditions. Class 1 represents recordings of seizure activity, while classes 2 to 5 represent non-seizure conditions (eyes open, eyes closed, healthy brain area, and area with a tumor). While the original dataset had 5 classes, class 1 (epileptic seizure) from the rest. (https://archive.ics.uci.edu/dataset/388/epileptic+seizure+recognition).

The input vector {1, 2, 3, 4, 5} has a column called "y" which represents the categories of the 178-dimensional input vector. This column provides information about the patient's eyes being open or closed, tumor location, and seizure activity. By analyzing the definitions of the different classes in column "y", to simplify the multi-classification task into a binary classification task. To group classes {2, 3, 4, 5} as 0, indicating "not epileptic seizure", while keeping class {1} as 1, representing an "epileptic seizure". It can also be used to localize and lateralize the brain activity during seizures to better understand the specific regions of the brain involved in epilepsy. This information is valuable for treatment planning of epilepsy.

Figure 2
The system model of Epilepsy classification and detection

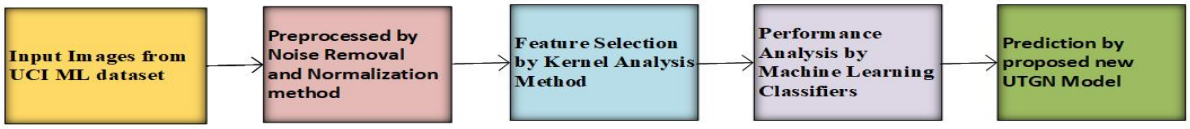

Figure 2 would include the following components: EEG data acquisition, pre-process to remove artifacts and noise, higher-level features selection based on time domain series, KCA algorithm was applied to identify the most informative features for epilepsy characteristics. The selected SVM, DBN, KNN, RF, DNN, KA-U-TGN classifier models are unique approach of learning patterns and making epilepsy predictions based on the extracted features. After the parameters are evaluated by model integration and fusion, the final prediction by displaying graphical representations, which helps for medical intervention.

3.2. Feature selection using kernel analysis (KCA):

Calculate the mean for each feature in the dataset by iterate over each feature. Next, subtract the mean value from each feature vector. This is done to remove the bias and center the data around zero. The covariance matrix is used to measure the relationship between different features in the dataset. The eigenvalue decomposition is performed to find the eigenvectors and eigenvalues of the covariance matrix. The eigenvectors represent the directions in which the data varies the most, while the eigenvalues correspond to the variance. Select the top k eigenvectors corresponding to the largest eigenvalues. These eigenvectors capture the most important features and can be used for dimensionality reduction. The dataset is projected onto the selected eigenvectors to obtain the reduced dimensional representation. This can be done by taking the dot product of the centered dataset and the selected eigenvectors. To obtain the reconstructed dataset, obtained by multiplied selected eigenvectors and add back the mean value. Finally, evaluate the performance of the feature selection using a performance metric of choice, such as classification accuracy or mean squared error. The selected features can be used for further analysis or modeling tasks.

Assuming a dataset C with dimensions N and d, we first get sample mean mj of the j-th feature as eq. (1)

$$m_j = \frac{1}{N}\sum_{i=1}^{N} C(i,j) \tag{1}$$

Following that, we determine zero-mean dataset B as eq. (2)

$$B = C - em^T \tag{2}$$

In this case, e stands for a N by 1 vector containing only ones. The Z covariance matrix is constructed in the third step as shown in eq. (3).

$$Z = \frac{B^*B}{N-1} \tag{3}$$

Fourth, the eigen decomposition expression for the covariance matrix Z is given by eq. (4)

$$Z = XYX^{-1} \tag{4}$$

Here, Y stands in for eigenvalue matrix, which is also a diagonal matrix, and X stands for the eigenvector matrix given in eq. (5).

$$Y = \begin{bmatrix} Y(1,1) & & \\ & Y(2,2) & \\ & & \ddots \\ & & Y(d,d) \end{bmatrix} \tag{5}$$

Fifth, X and Y are rearranged to make the eigenvalue decrease as shown in eq. (6).

$$Y(1,1) \geq Y(2,2) \geq \cdots \geq Y(d,d) \quad (6)$$

The sixth step is to determine the total variance for each eigenvector by eq. (7)

$$G(k) = \sum_{i=1}^{k} Y(i,i)$$

$$G = [G(1)G(2)\cdots G(d)] \quad (7)$$

Seventh, assuming T to be the threshold, we choose L* to satisfy given in eq. (8).

$$L^* = \arg\min \left\{ L | \frac{G(L)}{G(d)} \geq T \right\} \quad (8)$$

The most crucial principal component for L was produced. Kernel PCA (KPCA), a potent PCA version, has been presented by researchers as a solution to this issue. The KPCA uses the identical implementation as PCA with the exception of moving dataset C into a higher-dimensional space. There were two KPCAs examined. Polynomial kernel PCA (PKPCA), for example, is defined as eq. (9)

$$k(x,y|\text{PKPCA}) = [a(x \times y) + b]^c \quad (9)$$

where are the kernel parameters a, b, and c. RBF kernel PCA (RKPCA) is the alternative given by eq. (10).

$$k(x,y|\text{RKPCA}) = \exp\left(-\frac{\|x-y\|^2}{d^2}\right) \quad (10)$$

where d represents the scaling factor. In this section, convolutional neural network parameters, layers, and structure are discussed. A convolutional neural network (CNN) typically consists of three main layers: convolutional, pooling, and fully connected. It convolves the input image to make different component maps, and the network goes through two stages of training. In feed forward step input images are taken, each neuron's input and parameters are combined using a dot product, and a convolution operator is used in each layer. Network output is compared to desired output utilizing a loss function, and error rate before back propagation stage, which begins with error. This is repeated for a sufficient number of images. In order to preserve the same output size, zero-padding is applied to the input data. This is done consistently across all the convolutional layers in this study. By adding zeros to the information framework, the resulting grid size 4x4 remains unchanged. This ensures consistency in the structure of the neural network and supports image processing.

Initialization of weight: Network convergence can be accelerated with the right initial weights. The literature has presented a variety of weight initialization strategies. After examining the effects of various initializers, this study found that the "He" initializer with a normal distribution provides the best performance.

Function of activation: For the most part, a nonlinear administrator or enactment capability is utilized in profound establishments after convolutions. Presence of this capability model in correlation with a direct method in eq. (11).

$$\text{relu}\,(x) = \begin{cases} x & \text{if } x \geq 0 \\ 0 & \text{if } x < 0 \end{cases} \quad (11)$$

Leaky ReLU, as stated in (12), has frequently outperformed ReLU. When the function is not in use, it permits a tiny, non-zero gradient.

$$\text{leaky}_{\text{relu}\,(x)} = \begin{cases} x & \text{if } x \geq 0 \\ ax & \text{if } x < 0 \end{cases} \quad (12)$$

A = typically 0.3. The accuracy of classification and training speed have been improved by exponential linear units (ELUs). ELU accepts negative values, which enables it to more efficiently normalise mean unit activations towards zero than batch normalisation as shown in eq. (13).

$$\text{elu(x)} = \begin{cases} x & \text{if } x \geq 0 \\ a(e^x - 1) & \text{if } x < 0 \end{cases}\Big) \quad (13)$$

a = 1. Additionally, the effectiveness of the developing networks is evaluated when scaled exponential linear unit (SELU) activation function is present. The SELU is created by giving the ELU a little twist. Given below in eq. (14) are the equivalent equations for these functions, with a = 1.6732 and l = 1.0507.

$$\text{selu}(x) = \lambda \begin{cases} x & \text{if } x \geq 0 \\ ae^{x} - \alpha & \text{if } x < 0 \end{cases} \quad (14)$$

Pooling: When a convolutional layer is followed by a pooling layer, size of feature maps and number of parameters in network are reduced, resulting in lower computational costs. Because of adjoining pixels in computations, pooling layers are invariant to little changes. Max-pooling is one of the most widely utilized pooling strategies.

Regularization: Creation of a method that is effective not only with training data but also with new entries is the primary challenge in machine learning. For deep learning, a number of regularization strategies have been proposed. Dropout, a powerful but cost-effective computational regularization technique, is used in this paper. During the training phase, it randomly removes some of fully connected layer's nodes to prevent over-fitting. Then again, dropout is considered as a group technique, since it gives various organizations during preparing.

Dietary function: The choice of loss function that should be minimized is one of the most crucial aspects of designing a DNN (deep neural network). Typically, the categorical cross-entropy function (H), which was used in this case as shown in eq. (15).

$$H(p, q) = -\sum_{x} p(x) \ln\left(q(x)\right) \quad (15)$$

Algorithm of KCCA:

INPUT: Dataset
RESULT: The identification of neurological disorders is based on a number of factors.
Load the brain image dataset in the propased model
Pre-processing is used to remove undesined noise from an dataset.
Select features of pre-processed image
far each epoch in epoch Number do
for each bunch in balchised do
$y^{'}$ = model(feanires).
loss = crossEntropy $\left(y, y^{'}\right)$
whilet < Maximum number of iterations)
Adjust the revitalization velocities and positions to come up with new solutions.
if $r > s_y$)
At randiam, choose a solution from the best solutions.
Create a local solution that is close to the best-selected oprion.
end if
if $r < b_i \& f(x_i) < f($ Gbest))
Increase s_i and decrease b_i
end if
Rate the hats and identify the current Gbest
end while
acco:
$b^{*}Acc = \max(b^{*}Acc, acc)$;
Return

A convolutional neural network (CNN) typically consists of three main layers: convolutional, pooling, and fully connected. It convolves the input image to make different component maps, and the network goes through two stages of training. In feed forward step input images are taken, each neuron's input and parameters are combined using a dot product, and a convolution operator is used in each layer. Network output is compared to desired output utilizing a loss function, and error rate before back propagation stage, which begins with error. This is repeated for a sufficient number of images. In order to preserve the same output size, zero-padding is applied to the input data. This is done consistently across all the convolutional layers in this study. By adding zeros to the information framework, the resulting grid size 4x4 remains unchanged. This ensures consistency in the structure of the neural network and supports image processing.

3.3. Classification using proposed U-transfer Reinforced Gaussian networks (U-TRGN)

A fully connected CNN called U-Net is used for effective semantic segmentation. The U-Net deep neural network can be used for a wide range of analytical tasks. This is especially helpful in medical imaging. The U-Net design depends on an auto-encoder network, and it will duplicate its contributions to its results. U-Net contains two ways, a compression way (encoder) and a symmetric growing way (decoder). Transposed convolutions are used in the decoder path, allowing for precise localization. U-Net was initially intended for 572×572 pixels, it very well may be effectively altered to work with any image aspect. A few stacked convolutional layers are highlighted from the images, as shown in Figure. 3.

In this approach, the U-transfer reinforcement Gaussian networks (U-TRGN) are used for classification. The U-TRGN model is a combination of transfer learning and reinforcement learning techniques. First, the model used to extract features from the data. Next, the model applies a feature selection technique KCA to select the most relevant features from the UNet model output. KCCA is a statistical method that finds linear combinations of variables that have maximum correlation with the target variable. Once the features are selected, the U-TRGN model is trained, and provides an effective way to classify data by extracting relevant features using the UNet model, selecting the most informative features through KCA, and optimizing the classifier model. This approach combines the strengths of transfer learning, and feature selection, to achieve accurate and efficient classification of data.

Figure 3
U-TRAN architecture for the image classification model

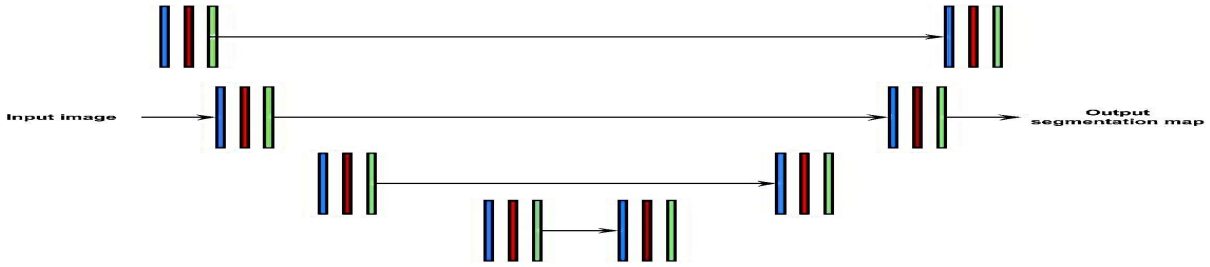

The efficient algorithm that makes reinforcement learning possible. The classification challenge that has been necessitates the sequential decision-making. The algorithm of multi-featured approach and a multilayer perceptron neural network is used in this study. The class labels of image converted in to source vector representation. The reward function depends on the state and action rather than the class. In each reinforcement learning (RL) formulation, the agent is an intuitive but formalized concept that acts in different states and receives specific rewards. The recommended set of actions that maximizes the overall expected cumulative reward received. Consequently, the ideal strategy for the specialist to follow. This scenario is defined by an image volume and a scalar number that shows whether prior class prediction (epilepsy vs. normal) was accurate. This prediction's accuracy is shown by pred_corr. It's described by eq. (16)

$$\text{pred\_corr} = \begin{cases} 1, \text{ if prediction is correct} \\ 0, \text{ if prediction is wrong.} \end{cases}$$

$$\text{pred\_corr} \equiv \delta_{a,l_{\text{XC}}} \tag{16}$$

where δ is the Kronecker delta function given by eq. (17).

$$s = \{\mathcal{M}, \text{pred\_corr}\}, \tag{17}$$

To downsize the x and y plane from original image size to 64 x 64 pixels in order to make all matrices same size and make 3D convolutional back propagation easier to compute. Moreover, having various quantities of cuts for the different pictures (going from 28 to 36), we make the z-tomahawks of equivalent length by adding no lattices of size 64 × 64 pixels to caudal piece of pictures, so that all have z-aspect of 36. In essence, this is padding in z-direction. Two possible actions, a1 and a2, are simply prediction of whether image M is normal or epilepsy containing as shown in eq. (18),

$$\mathcal{A} = \begin{pmatrix} a_1 \\ a_2 \end{pmatrix} = \begin{pmatrix} 0 \\ 1 \end{pmatrix} = \begin{pmatrix} \text{predict normal} \\ \text{predict epilepsy} \end{pmatrix} \tag{18}$$

The incentivizes used to promote accurate class predictions. As a result, to reward a correct forecast with +1 and penalise a bad prediction with a reward of -1. The reward r can be defined in terms of prediction accuracy, pred_corr by eq. (19):

$$r = \begin{cases} -1, \text{if pred\_corr } = 0 \\ +1, \text{if pred\_corr } = 1. \end{cases} \tag{19}$$

In RL, the action-value function, indicated by Q (s, a), is a crucial element. An "episode" is a collection of states where an agent restarts in a different state. Action-value function shows the anticipated cumulative reward if, after doing action, a predetermined process for choosing actions is followed until the end of the episode. The relevant action-value, Q (s, a), for a particular policy, is defined by eq. (20):

$$Q^{\pi}(s,a) = E_{\pi}\{R_t | s_t = s, a_t = a\} = E_{\pi}\left\{\sum_{k=0}^{\infty} \gamma^k r_{t+k+1} | s_t = s, a_t = a\right\} \tag{20}$$

where ERt|st = s, at = an is expectation for Rt upon choosing action an in-state s and subsequently choosing actions in accordance with, and Rt is total cumulative reward commencing at time t. The weighting of "instant gratification" versus "delayed gratification" is represented by the discount factor of 0.99. By maximising it, the action-value function is crucial, and eventually arrive the desired behaviour, leads to an accurate image class prediction. Two-node output depicts the two possible action-values, Q (s, a1) and Q (s, a2), that can be obtained by acting on state- s in either of two different ways as shown in eq. (21).

$$p(x) = \sum_{j=1}^{K} \pi_j p\left(x; \theta_j\right),\ j = 1, \ldots, K.$$

$$p(\mathbf{x}) = \sum_{c=1}^{C} \pi_c f_c(\mathbf{x}|\theta) \tag{21}$$

Mixture model has a vector of parameters, $\underline{\theta} = \{\theta_1, \ldots, \theta_k, \pi_1, \ldots \pi_k\}$

Hidden variables are treated as a latent variable, or Z, in mixture models. It accepts numbers 1 through K as a discrete set that satisfies the conditions $z_k \epsilon \{0,1\}$ and $\sum_z z_k = 1$. A conditional distribution p (x | z) and a marginal distribution p (z) are how we define the joint distribution p (x, z) given by eq. (22).

$$p(z,x) = p(z)p(x|z)$$

$$p(z_k = 1) = \pi_k \tag{22}$$

A definition of probability density function of X in eq. (23)

$$p(x|\mu_k, \Sigma_k) = \frac{1}{\sqrt{2\pi|\Sigma^{-1}|}} \exp\left(-\frac{1}{2}(x-\mu_x)\Sigma_x^{-1}(x-\mu_x)^T\right)$$

$$f_c(\mathbf{x}|\boldsymbol{\mu}_c, \boldsymbol{\Sigma}_c) = \frac{1}{(2\pi)^{\frac{d}{2}}|\boldsymbol{\Sigma}_c|^{\frac{1}{2}}} \exp\left(-\frac{1}{2}(\mathbf{x}-\boldsymbol{\mu}_c)^t \boldsymbol{\Sigma}_c^{-1}(\mathbf{x}-\boldsymbol{\mu}_c)\right) \tag{23}$$

A linear superposition of Gaussians is utilized to represent a Gaussian mixture distribution in the form by eq. (24),

$$p(x) = \sum_{k=1}^{K} \pi_k p(x|\mu_k, \Sigma_k)$$

$$\hat{\pi}_c = \frac{n_c}{n},$$

$$\hat{\mu}_c = \frac{1}{n_c}\sum_{\{f|y_i=c\}}\mathbf{x}_i$$

$$\hat{\mathbf{\Sigma}}_c = \frac{1}{(n_c-1)}\sum_{\{i|y,=c\}}(\mathbf{x}_i - \boldsymbol{\mu}_c)(\mathbf{x}_i - \boldsymbol{\mu}_c)^t \quad (24)$$

Given a certain value of z, conditional distribution of x is now a Gaussian by eq. (25):

$$p(x|z_k = 1) = p(x|\mu_k, \Sigma_k)$$

$$p(x|z) = \prod_{k=1}^{K} p(x|\mu_k, \Sigma_k)^{z_k} \quad (25)$$

By adding joint distribution of all possible states of z, one can obtain the marginal distribution of x given in eq. (26).

$$p(x) = \sum_z p(z)p(x|z) = \sum_{k=1}^{K} \pi_k p(x|\mu_k, \Sigma_k) \quad (26)$$

The "posterior probability" on a mixture component for a certain data vector is a significant derived quantity by eq. (27):

$$\gamma(z_k) \equiv p(z_k = 1|x) = \frac{p(z_k=1)p(x|z_k=1)}{\sum_{j=1}^{K} p(z_j=1)p(x|z_j=1)} = \frac{\pi_k p(x|\mu_k,\Sigma_k)}{\sum_{j=1}^{K}\pi_j p(x|\mu_j,\Sigma_j)} \quad (27)$$

Again, to maximise Q (s, a) in order to maximise the overall cumulative benefit by selecting the argmax (Q), which was used to find the largest probability class prediction. In order to estimate the function for Qt(a), the Deep Q network (DQN) was used. It employs 3 X 3 kernels with a stride of 2 and padding, producing the same filter sizes as before. In contrast to support advancement, Q (s, a) stands out as the activity esteem capability. With a learning rate of 1104 and n batch = 16, with mean squared error rate. The difference between the output Q values, QDQN, and the "target" Q value, Q target, constitutes our DQN loss. The first one is calculated using a forward pass: Q (t) DQN = FDQN (st) of DQN. In order to ensure that QDQN is as generally applicable as possible, batches of batch size. The n batch transitions are randomly selected from T during DQN training. This allows for an extensive and evenly distributed sampling of states and surroundings. The test for N episodes = 300 episodes overall, each of which consists of five progressive expressions and all of which begin with s1, which is randomly selected for each episode among 10 preparation sets.

3.4. Performance analysis

The recommended approach is executed on a Windows 10 center i7-4710MQ computer chip running at 2.5 GHz (8 central processors), with 8 GB of Slam and 1 GB of committed illustrations handling unit memory. All experiments are performed on a Personal computer with Intel Core i5 GH z processor and 8.00 GB RAM, nvidia. The proposed method is implemented in Python 3.6.5.

The confusion matrix was analyzed in terms of true and false positives and negatives. Accuracy was calculated by dividing the total number of correct predictions (true positives + true negatives) by the total number of samples (positives + negatives). The Dice score was used to measure the number of true positives as well as false positives.

$$\text{Accuracy}=\frac{(TP+TN)}{(TP+FP+TN+FN)},\text{Precision}=\frac{(TP)}{(TP+FP)},\text{Recall}=\frac{(TP)}{(TP+FN)},\ \text{DSC} = 2\frac{|X\cap Y|}{|X|+|Y|} = \frac{2TP}{2TP+FN+FP} = 2\frac{\text{Precision}\times\text{Recall}}{\text{Precision}+\text{Recall}}.$$

The performance was evaluated by randomized method of "train and test" approach. The classification results for the training and test data sets are evaluated by confusion matrix. in figure-4 (a), (b). this shows the actual and predicted class for detection of epilepsy for training and test dataset. Based on this confusion matrix the precision recall curve is obtained by training and testing dataset for this actual and predicted class of epilepsy detection as shown in figure 4 has the convergence of fitness over iteration, figure 5 has training and testing accuracy and loss, figure 6 explains confusion matrix, figure 7 and figure 8 shows the ROC and PR curve is analysed based on this confusion matrix.

Figure 4
Convergence of Fitness over 25- Iteration and 5-KCCA agents

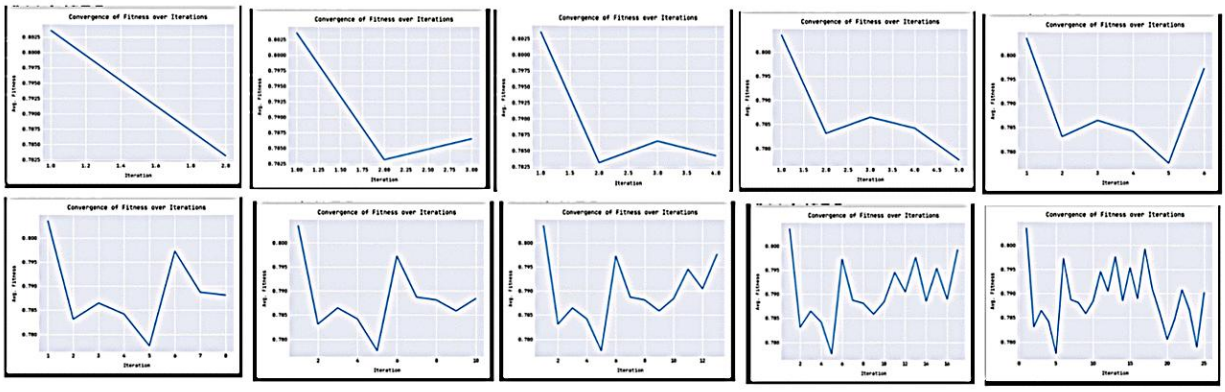

Figure 5
Training and Testing accuracy and loss

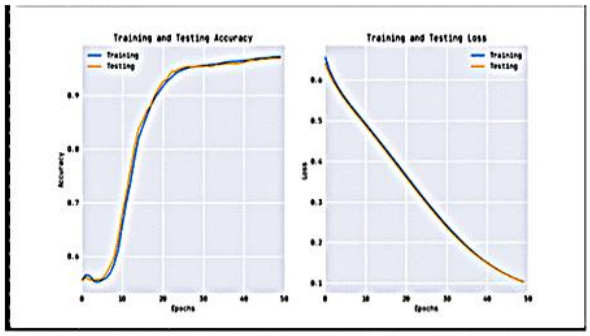

Figure 6
Confusion matrix

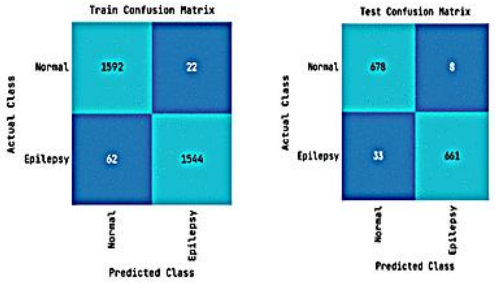

Figure 7
ROC curve

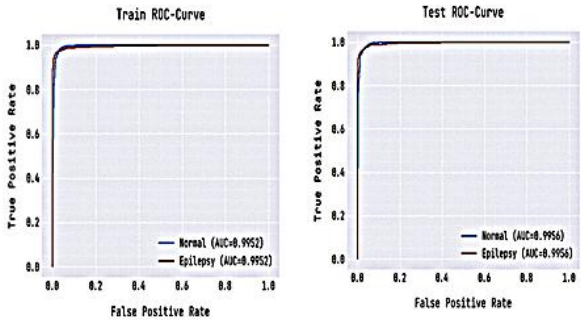

Figure 8
PR curve of epilepsy

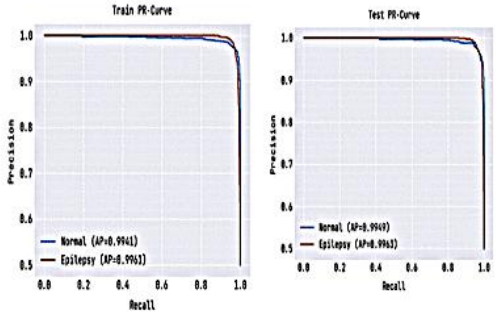

Table 1
Proposed analysis based on training and testing dataset

Metrics	Training results in %	Testing results in %
Accuracy	97.39	97.04
Precision	94.81	94.12
Dice coefficient	2.61	2.96
AUC	99.52	99.56

The above table-1 shows training and testing dataset based on proposed analysis in terms of accuracy. Accuracy is used to evaluate the overall performance by classified instances out of the total instances. A higher accuracy gives better model performance, dice co-efficient gives the similarity between 2 set of data (0 or 1). A higher precision value gives a low false positive rate. AUC assessed by binary classification method.

Figure 9
Comparison graph on different classifiers models

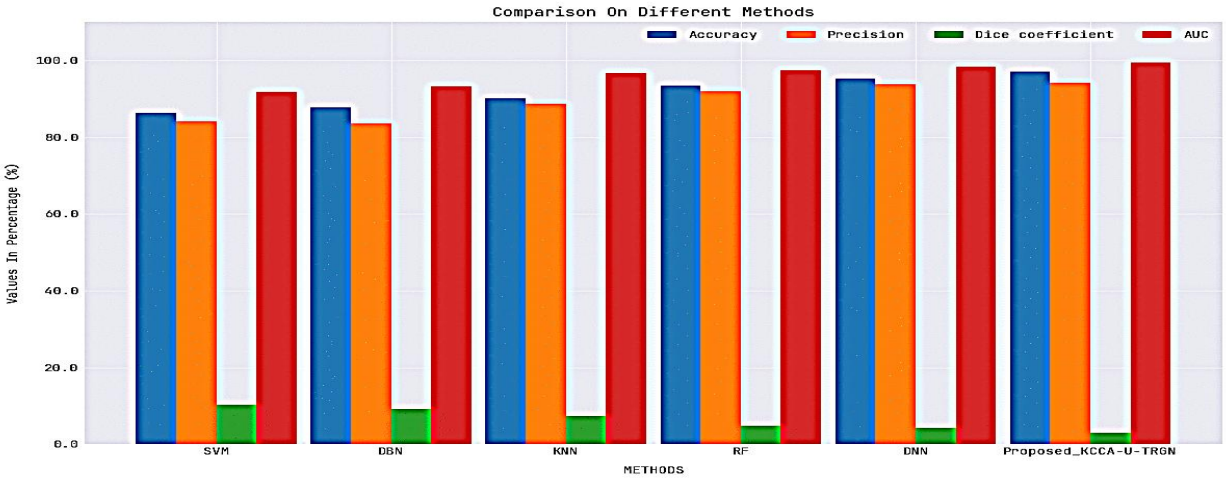

Figure 10
Comparison graph on different performance levels

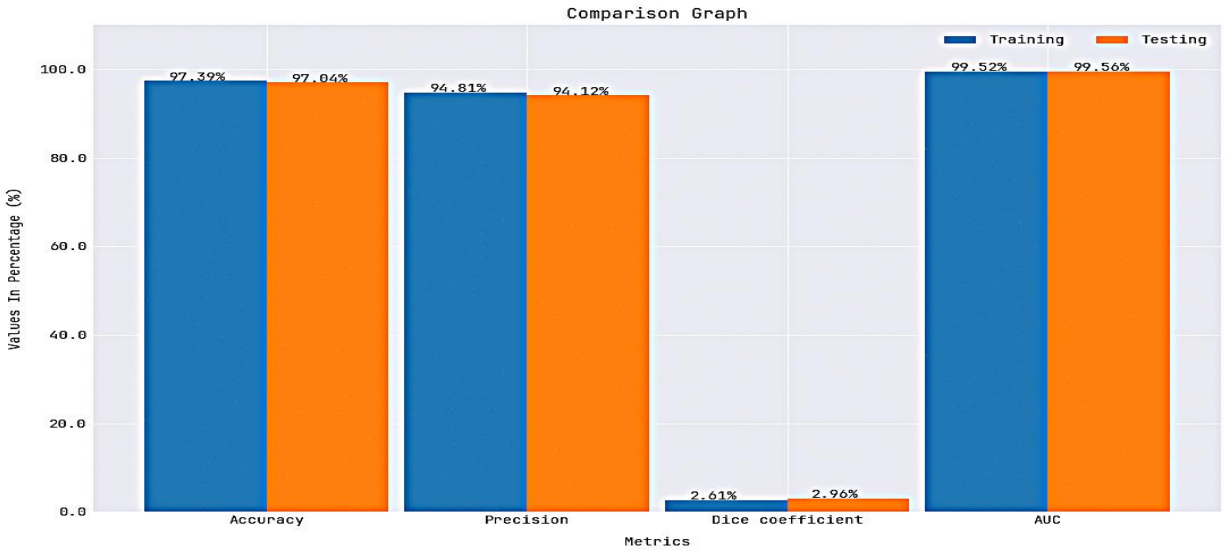

The Precision, Dice coefficient, AUC. Here proposed technique attained accuracy of 97.39%, Precision of 94.81%, Dice coefficient of 2.61, AUC of 99.52% for training dataset; for testing dataset, proposed technique with different classifier models is attained accuracy of 97.04%, Precision of 94.12%, Dice coefficient of 2.96%, AUC of 99.56% as shown in figure 9 and figure 10.

Table 2
Comparative analysis based on existing and proposed analysis

Metrics	SVM	DBM	KNN	RF	DNN	Proposed- KA-U-TGN
Accuracy	86.34	87.77	90.23	93.45	95.21	97.04
Precision	84.12	83.56	88.78	91.91	93.84	94.12
Dice coefficient	10.2	9.12	7.32	4.86	4.23	2.96
AUC	91.89	93.22	96.83	97.45	98.43	99.56

Table-2 shows analysis based on training and testing dataset. Existing technique compared are SVM, DBM, KNN, RF, DNN with proposed model. Proposed technique attained accuracy of 97.04%, Precision of 94.12%, Dice coefficient of 2.96%, AUC of 99.56%.

The recent existing studies are clearly showing the deep feature maps from convolutional neural networks are utilized in shallow classifiers to identify anomalies by reducing dimensionality through Principal Component Analysis (PCA)-Bonn dataset. The algorithm categorizes preictal and interictal segments of patients using patient-specific features, removing the need for manual feature extraction. When tested on open-source epilepsy datasets, it achieved a sensitivity of 82% and a false prediction rate of 0.19. The deep learning system for automatically detecting and distinguishing spontaneous seizures, improving model performance and interpretability by recognizing biologically meaningful features in EEG. The deep network model based on ResNet theory and LSTM for classifying seizure types from EEG trials, surpassing other models with an F1-score of 97.4%. The method achieves RF classifier achieving 97.96% accuracy and the MLP classifier achieving 98.98% accuracy. The AI and IoT-based seizure detection, and presents opportunities and future research directions. This article provides a comprehensive overview of different modalities, discusses seizure detection processes reviews, and the new UTRGN deep learning model increased performance[45-50].

4. Conclusion

The proposed technique in epilepsy detection aids in selecting the processed brain signal using kernel convolutional component analysis (KCA) and the selected features are classified using U-Transfer Reinforced Gaussian networks (U-TRGN). Choosing the most relevant clinical variables could improve classifier performance and reduce dimensionality in small sample with specific characteristics, through the elimination of irrelevant features to increase the performance. These selected features are likely influenced by the decision to undergo surgery, with reduced predictor variables. In the combination of PET and X-ray features, the indicator variables offer limited information about the temporal areas of hypo metabolism. The precise physical locations of excisions within the hippocampus, amygdala piriform cortex complex, and entorhinal cortex have been found to have a significant correlation with seizure outcomes. If these areas are targeted for surgical intervention, there is a noticeable impact on reducing epileptic seizures. To identify the anatomical regions by AI models used to optimize surgical strategies and improve patient outcomes.

Conflicts of Interest

The authors declare that they have no conflicts of interest to this work.

References

1.Chang, A. J., Roth, R., Bougioukli, E., Ruber, T., Keller, S. S., Drane, D. L., ... & Alzheimer′s Disease Neuroimaging Initiative. (2023). MRI-based deep learning can discriminate between temporal lobe epilepsy, Alzheimer ′ s disease, and healthy controls. Communications Medicine, 3(1), 33.

2.Joon Y. Kang, Chengyuan Wu, Laser interstitial thermal therapy for medically intractable mesial temporal lobe epilepsy, Epilepsia,First published: 24 December 2015, https://doi.org/10.1111/epi.13284

3.Sinclair, B., Cahill, V., Seah, J., Kitchen, A., Vivash, L. E., Chen, Z., ... & O'Brien, T. J. (2022). Machine learning approaches for imaging ‐ based prognostication of the outcome of surgery for mesial temporal lobe epilepsy. Epilepsia, 63(5), 1081-1092.

4.Sakashita, K., Akiyama, Y., Hirano, T., Sasagawa, A., Arihara, M., Kuribara, T., ... & Mikuni, N. (2023). Deep learning for the diagnosis of mesial temporal lobe epilepsy. Plos one, 18(2), e0282082.

5.Garcia-Ramos, C., Nair, V., Maganti, R., Mathis, J., Conant, L. L., Prabhakaran, V., ... & Struck, A. F. (2022). Network phenotypes and their clinical significance in temporal lobe epilepsy using machine learning applications to morphological and functional graph theory metrics. Scientific Reports, 12(1), 14407.

6.Akrami, H., Leahy, R. M., Irimia, A., Kim, P. E., Heck, C. N., & Joshi, A. A. (2022). Neuroanatomic Markers of Posttraumatic Epilepsy Based on MR Imaging and Machine Learning. American Journal of Neuroradiology, 43(3), 347-353.

7.Meng, X., Deng, K., Huang, B., Lin, X., Wu, Y., Tao, W., ... & Chen, F. (2023). Classification of temporal lobe epilepsy based on neuropsychological tests and exploration of its underlying neurobiology. Frontiers in Human Neuroscience, 17, 1100683.

8.Sayed, N.M., Aldin, M.T.K., Ali, S.E. et al. Cognitive functions and epilepsy-related characteristics in patients with generalized tonic−clonic epilepsy: a cross-sectional study. Middle East Curr Psychiatry 30, 15 (2023). https://doi.org/10.1186/s43045-023-00293-6.

9.Aronica, E. Gliomas and epilepsy: Insights from neuropathological studies in humans. SpringerPlus 4 (Suppl 1), L9 (2015). https://doi.org/10.1186/2193-1801-4-S1-L9

10.Elbeh, K.A.M., Elserogy, Y.M., Hamid, M.F. et al. Personality traits in patients with refractory versus non-refractory epilepsy. Middle East Curr Psychiatry 28, 27 (2021). https://doi.org/10.1186/s43045-021-00106-8

11.Al-Malt, A.M., Abo Hammar, S.A., Rashed, K.H. et al. The effect of nocturnal epileptic seizures on cognitive functions in children with idiopathic epilepsy. Egypt J Neurol Psychiatry Neurosurg 56, 49 (2020). https://doi.org/10.1186/s41983-020-00182-3

12.Güvenç, C., Dupont, P., Van den Stock, J. et al. Correlation of neuropsychological and metabolic changes after epilepsy surgery in patients with left mesial temporal lobe epilepsy with hippocampal sclerosis. EJNMMI Res 8, 31 (2018). https://doi.org/10.1186/s13550-018-0385-5

13.Abdelgawad, E.A., Mounir, S.M., Abdelhay, M.M. et al. Magnetic resonance imaging (MRI) volumetry in children with nonlesional epilepsy, does it help? Egypt J Radiol Nucl Med 52, 35 (2021). https://doi.org/10.1186/s43055-021-00409-0

14.Faheem, M.H., Dabour, A.S. & Abdelhaie, O.M. Diagnostic and prognostic role of proton single-voxel spectroscopy (SVS) in non-lesional epilepsy pediatric patients: prospective controlled study. Egypt J Radiol Nucl Med 51, 143 (2020). https://doi.org/10.1186/s43055-020-00251-w

15.Luckett, P. H., Maccotta, L., Lee, J. J., Park, K. Y., UF Dosenbach, N., Ances, B. M., ... & Leuthardt, E. C. (2022). Deep learning resting state functional magnetic resonance imaging lateralization of temporal lobe epilepsy. Epilepsia, 63(6), 1542-1552.

16.Wang, J., Guo, K., Cui, B., Hou, Y., Zhao, G., & Lu, J. (2022). Individual [18F] FDG PET and functional MRI based on simultaneous PET/MRI may predict seizure recurrence after temporal lobe epilepsy surgery. European Radiology, 32(6), 3880-3888.

17.Ruowei, Q., Shifen, W., Zhengfang, L., Junhua, G., & Guizhi, X. (2022). 3D-CNN frameworks for mesial temporal lobe epilepsy diagnosis in MRI images. International Journal of Applied Electromagnetics and Mechanics, 70(4), 515-523.

18.Vorndran, J., Neuner, C., Coras, R. et al. A deep learning-based histopathology classifier for Focal Cortical Dysplasia. Neural Comput & Applic 35, 12775−12792 (2023). https://doi.org/10.1007/s00521-023-08364-9

19.Pisano, B., Teixeira, C.A., Dourado, A. et al. Application of self-organizing map to identify nocturnal epileptic seizures. Neural Comput & Applic 32, 18225−18241 (2020). https://doi.org/10.1007/s00521-019-04327-1

20.Raab, D., Theissler, A. & Spiliopoulou, M. XAI4EEG: spectral and spatio-temporal explanation of deep learning-based seizure detection in EEG time series. Neural Comput & Applic 35, 10051−10068 (2023). https://doi.org/10.1007/s00521-022-07809-x

21.Raghu, S., Sriraam, N., Vasudeva Rao, S. et al. Automated detection of epileptic seizures using successive decomposition index and support vector machine classifier in long-term EEG. Neural Comput & Applic 32, 8965 − 8984 (2020). https://doi.org/10.1007/s00521-019-04389-1

22.Glory, H.A., Vigneswaran, C., Jagtap, S.S. et al. AHW-BGOA-DNN: a novel deep learning model for epileptic seizure detection. Neural Comput & Applic 33, 6065−6093 (2021). https://doi.org/10.1007/s00521-020-05384-7

23.Mendonça, F., Fred, A., Mostafa, S.S. et al. Automatic detection of cyclic alternating pattern. Neural Comput & Applic 34, 11097−11107 (2022). https://doi.org/10.1007/s00521-018-3474-5

24.Raghu, S., Sriraam, N., Vasudeva Rao, S. et al. Automated detection of epileptic seizures using successive decomposition index and support vector machine classifier in long-term EEG. Neural Comput & Applic 32, 8965 − 8984 (2020). https://doi.org/10.1007/s00521-019-04389-1

25.Glory, H.A., Vigneswaran, C., Jagtap, S.S. et al. AHW-BGOA-DNN: a novel deep learning model for epileptic seizure detection. Neural Comput & Applic 33, 6065−6093 (2021). https://doi.org/10.1007/s00521-020-05384-7

26.Mendonça, F., Fred, A., Mostafa, S.S. et al. Automatic detection of cyclic alternating pattern. Neural Comput & Applic 34, 11097−11107 (2022). https://doi.org/10.1007/s00521-018-3474-5

27.Siddiqui, M.K., Islam, M.Z. & Kabir, M.A. A novel quick seizure detection and localization through brain data mining on ECoG dataset. Neural Comput & Applic 31, 5595−5608 (2019). https://doi.org/10.1007/s00521-018-3381-9

28.N. Dang, K. Shao, L. Chen and M. Yang, "Multi-model decision-making seizure types classification based on transfer learning," 2022 International Symposium on Control Engineering and Robotics (ISCER), Changsha, China, 2022, pp. 192-201, doi: 10.1109/ISCER55570.2022.00040.

29.Kang, L., Chen, J., Huang, J., Zhang, T., & Xu, J. (2022). Identifying epilepsy based on machine‐learning technique with diffusion kurtosis tensor. CNS Neuroscience & Therapeutics, 28(3), 354-363.

30.Zhang, Y., Zhang, D., Chen, Z., Wang, H., Miao, W., & Zhu, W. (2022). Clinical evaluation of a novel atlas-based PET/CT brain image segmentation and quantification method for epilepsy. Quantitative Imaging in Medicine and Surgery, 12(9), 4538.

31.Debicki, D. B., (2017). Electroencephalography after a single unprovoked seizure. Seizure, 49, 69-73. https://doi.org/10.1016/j.seizure.2017.03.001

32.ANDREAS MILTIADOUS, KATERINA, D., TZIMOURTA, (2023). Machine Learning Algorithms for Epilepsy Detection Based on Published EEG Databases: A Systematic Review, IEEE Access, version 3,doi. 10.1109/ACCESS.2022.3232563

33.Ijaz Ahmad,Xin Wang,Mingxing Zh.(2022)EEG-Based Epileptic Seizure Detection via Machine/Deep Learning Approaches: A Systematic Review, computational intelligence and Neuro Sciencehttps://doi.org/10.1155/2022/6486570

34.Xiong, Z., Wang, H., Zhang, L., Fan, T., Shen, J., Zhao, Y., Liu, Y., & Wu, Q. (2020). A Study on Seizure Detection of EEG Signals Represented in 2D. Sensors, 21(15), 5145. https://doi.org/10.3390/s21155145

35.HU, J., MO, J., CHENG, X. (2023). Microglial TRPV1 in epilepsy: Is it druggable for new antiepileptic treatment? BIOCELL, 47(8), 1689–1701.

36.Cheng, Z., Tao, Y., Gu, X., Jiang, Y., Qian, P. (2023). Cross-Domain TSK Fuzzy System Based on Semi-Supervised Learning for Epilepsy Classification. CMES-Computer Modeling in Engineering & Sciences, 137(2), 1613–1633.

37.J. Wang, B. Li, C. Qiu, X. Zhang, Y. Cheng et al., "multi-view & transfer learning for epilepsy recognition based on eeg signals," Computers, Materials & Continua, vol. 75, no.3, pp. 4843–4866, 2023.

38.J. Qiang Wang, W. Fang and V. S. Sheng, "Prediction of epileptic eeg signal based on secnn-lstm," Journal of New Media, vol. 4, no.2, pp. 73–84, 2022.

39.S. Beatrice and J. Meena, "Overhauled approach to effectuate the amelioration in eeg analysis," Intelligent Automation & Soft Computing, vol. 33, no.1, pp. 331–347, 2022.

40.S. Bayrak, E. Yucel and H. Takci, "Epilepsy radiology reports classification using deep learning networks," Computers, Materials & Continua, vol. 70, no.2, pp. 3589–3607, 2022.

41.S. Naseem, K. Javed, M. Jawad Khan, S. Rubab, M. Attique Khan et al., "Integrated cwt-cnn for epilepsy detection using multiclass eeg dataset," Computers, Materials & Continua, vol. 69, no.1, pp. 471–486, 2021.

42.S. Majed Alotaibi, A., M. Imran Basheer and M. Adnan Khan, "Ensemble machine learning based identification of pediatric epilepsy," Computers, Materials & Continua, vol. 68, no.1, pp. 149–165, 2021.

43.S. Cherukuvada and R. Kayalvizhi, "Feature selection with deep belief network for epileptic seizure detection on eeg signals," Computers, Materials & Continua, vol. 75, no.2, pp. 4101–4118, 2023.

44.J. Liu, Y. Du, X. Wang, W. Yue and J. Feng, "Automated machine learning for epileptic seizure detection based on eeg signals," Computers, Materials & Continua, vol. 73, no.1, pp. 1995–2011, 2022.

45.Zeng, W., Shan, L., Su, B., & Du, S. (2023). Epileptic seizure detection with deep EEG features by convolutional neural network and shallow classifiers. Frontiers in Neuroscience, 17, 1145526. https://doi.org/10.3389/fnins.2023.1145526

46.Ibrahim, A. K., Zhuang, H., Tognoli, E., Muhamed Ali, A., & Erdol, N. (2023). Epileptic seizure prediction based on multiresolution convolutional neural networks. Frontiers in Signal Processing, 3, 1175305. https://doi.org/10.3389/frsip.2023.1175305

47.Statsenko, Y., Babushkin, V., Talako, T., Kurbatova, T., Smetanina, D., Simiyu, G. L., Habuza, T., Ismail, F., Almansoori, T. M., Gorkom, K. N., Szólics, M., Hassan, A., & Ljubisavljevic, M. (2023). Automatic Detection and Classification of Epileptic Seizures from EEG Data: Finding Optimal Acquisition Settings and Testing Interpretable Machine Learning Approach. Biomedicines, 11(9), 2370. https://doi.org/10.3390/biomedicines11092370

48.Alshaya, H., & Hussain, M. (2022). EEG-Based Classification of Epileptic Seizure Types Using Deep Network Model. Mathematics, 11(10), 2286. https://doi.org/10.3390/math11102286

49.Alalayah, K. M., Senan, E. M., Atlam, H. F., Ahmed, I. A., & Ahmad Shatnawi, H. S. (2023). Effective Early Detection of Epileptic Seizures through EEG Signals Using Classification Algorithms Based on t-Distributed Stochastic Neighbor Embedding and K-Means. Diagnostics, 13(11). https://doi.org/10.3390/diagnostics13111957

50.Ein Shoka, A. A., Dessouky, M. M., El-Sayed, A., & El-Din Hemdan, E. EEG seizure detection: Concepts, techniques, challenges, and future trends. Multimedia Tools and Applications, 1-31. https://doi.org/10.1007/s11042-023-15052-2